Journal of Wind Engineering & Industrial Aerodynamics 190 (2019) 40–52

Contents lists available at ScienceDirect

Journal of Wind Engineering & Industrial Aerodynamics

journal homepage: www.elsevier.com/locate/jweia

Performance-based bi-objective design optimization of wind-excited building systems

Arthriya Suksuwan, Seymour M.J. Spence *

Department of Civil and Environmental Engineering, University of Michigan, Ann Arbor, MI 48109, USA

ARTICLE INFO

Keywords:
Bi-objective optimization
Performance-based design
Wind engineering
System-level loss assessment
Monte Carlo simulation
Stochastic wind loads
High-dimensional problems
Kriging metamodeling

ABSTRACT

This paper proposes a framework for the bi-objective optimization of uncertain and dynamic wind-excited systems whose susceptibility to system-level damage is modeled through probabilistic fragility-based loss measures. In particular, the proposed framework is based on first reformulating the bi-objective stochastic optimization problem into a suite of single-objective optimization problems through the ε-constraint approach. Secondly, a new optimization sub-problem is introduced for efficiently solving the single-objective problems, whose formulation is based on combining the auxiliary variable vector approach with a new kriging-enhanced approximation scheme. Because the sub-problem can be fully calibrated and subsequently solved from the results of a single performance assessment carried out in a fixed point of the design space, efficiency and scalability to high-dimensional problems is achieved. Through solving a sequence of sub-problems, solutions to the ε-constraint problems are obtained leading to the identification of the Pareto-optimal solutions of the original bi-objective optimization problem. To illustrate the applicability, efficiency and scalability of the proposed framework, an example of application to a large-scale structure is presented, where structural material volume and a system-level loss measure defined in terms of expectation and standard deviation of the total repair cost are simultaneously minimized.

1. Introduction

The identification of structural designs that simultaneously minimize the initial cost of the system together with anticipated losses from damage due to extreme events defines a typical bi-objective optimization problem. Due to the inherently conflicting nature of these two objectives, strategies are needed that provide, as an output, a suite of Pareto-optimal solutions, among which the decision-makers can then choose the preferred option, i.e. design. In the context of performance-based wind engineering, if the applicability to structures of practical interest is sought, such optimization strategies have to be able to deal with high-dimensional vectors of design variables and computationally intensive stochastic (e.g. Monte Carlo) simulation-based performance assessment models. Indeed, due to their generality, most modern performance-based wind engineering frameworks are based on propagating uncertainty through complex response, damage and loss models by means of stochastic simulation (e.g. Barbato et al., 2013; Bernardini et al., 2012, 2015a; Chuang and Spence, 2017; Ierimonti et al., 2017, 2018; Cui and Caracoglia, 2018; Bezabeh et al., 2018; Zheng et al., 2019; Ouyang and Spence, 2019). An important consequence of this is that direct approaches for solving the bi-objective optimization problem through genetic algorithms (e.g. Liu et al., 2005; Fragiadakis et al., 2006; Bocchini and Frangopol, 2012; Gencturk, 2013; Saadat et al., 2014; Garcıa-Segura et al., 2017; Xu et al., 2017) are not easily applicable due to their need to evaluate system performance hundreds, if not thousands, of times before convergence. To overcome this difficulty, methods have recently been proposed based on building metamodels of the probabilistic performance measures in the augmented space of the design and uncertain parameters (Gidaris and Taflanidis, 2015; Gidaris et al., 2018). While this approach is extremely robust in terms of the systems it can treat, e.g. general nonlinear systems, it is not easily applicable to problems with high-dimensional vectors of design variables due to how this significantly increases the computational effort required to build the metamodels. This issue also effects approaches based on building metamodels directly in the space of the design variables (e.g. Bernardini et al., 2015b; Elshaer and Bitsuamlak, 2018; Ding and Kareem, 2018; Muñoz Paniagua and García, 2019). Alternatively, bi-objective optimization problems may be reformulated (scalarized) to enable the use of single-objective optimization algorithms. One of the most popular scalarization strategies is the ε-constraint method (e.g. Carmichael, 1980; Fu and Frangopol, 1990; Mavrotas, 2009; Zhang and Reimann, 2014), where a chosen objective is optimized, using a single-objective method, while the other objective

* Corresponding author.
E-mail addresses: arthriya@umich.edu (A. Suksuwan), smjs@umich.edu (S.M.J. Spence).

https://doi.org/10.1016/j.jweia.2019.03.028
Received 1 September 2018; Received in revised form 27 March 2019; Accepted 27 March 2019
Available online 20 April 2019
0167-6105/© 2019 Elsevier Ltd. All rights reserved.

functions are used as constraints. Differently from other methods based on combining the various objective functions into one single function (such as the weighted sum method), this approach does not require an *a priori articulation of preference* (Marler and Arora, 2004) from the decision-makers and, by using different thresholds for the constraint, yields a Pareto-optimal set of solutions. The effectiveness of the scalarization method depends, however, on the capability of the embedded single-objective optimization algorithm of handling the aforementioned challenges, i.e. high-dimensional vectors of design variables coupled with estimating performance through stochastic simulation. While several simulation-based design optimization methods have been proposed that can treat problems in high-dimensional uncertain spaces (e.g. Zou and Mahadevan, 2006; Jensen et al., 2008; Taflanidis and Beck, 2009; Jensen et al., 2012; Jia and Taflanidis, 2013; Jia et al., 2015), methods that can treat high-dimensional design spaces are very limited (Valdebenito and Schuëller, 2010). A method that can simultaneously handle high-dimensional design and uncertain spaces together with system-level probabilistic constraints has been proposed in (Suksuwan and Spence, 2018a, b). However, the performance functions of the aforementioned method are strictly limited to structural responses, notwithstanding the need to translate structural behavior into loss measures that are meaningful to the decision-makers and the society.

This work is focused on the development of a novel bi-objective optimization framework that can handle problems involving system-level probabilistic loss measures that are assessed in terms of fragility functions, high-dimensional spaces of design variables, and uncertain dynamic systems driven by stochastic wind excitation. The basic idea behind the framework is to first reformulate the bi-objective optimization problem through the ε-constraint approach. A new sequential kriging-enhanced optimization model is then introduced for efficiently solving each ε-constraint problem. Because the kriging-enhanced sequential approximation scheme at the core of the sub-problem is defined in the space of the second order statistics of the demand parameters, scalability to high-dimensional spaces of design variables and random variables is achieved. An example of application to a large-scale wind-excited system is presented to demonstrate the effectiveness and efficiency of the proposed framework.

2. Problem setting

2.1. The bi-objective design optimization problem

The problem of interest to this work is the optimization of structural systems subject to stochastic wind excitation, where two competing objectives are considered: the minimization of the initial cost and the minimization of the anticipated wind-induced losses. The problem is therefore to identify the solutions that represent the best trade-offs between these two needs. As such, it can be posed in the form of the following bi-objective design optimization problem:

$$\begin{array}{ll} \text{Find} & \mathbf{x} = \{x_1, \dots, x_N\}^T \\ \text{to minimize} & [V(\mathbf{x}), L(\mathbf{x})] \\ \text{subject to} & x_n \in \mathbb{X}_n \quad n = 1, \dots, N \end{array} \tag{1}$$

where $\mathbf{x}$ is a design variable vector containing the N deterministic parameters used to define the structural system (e.g. member sizes); V represents a function associated with the initial cost of the structural system (e.g. structural material volume); L is a function defining a system-level loss measure for a windstorm of given intensity (e.g. the expected value of the repair cost); and $\mathbb{X}_n$ is the set of values that the nth component of the design variable vector can assume. Since the two objectives in Eq. (1) are competing, the optimization will provide a set of Pareto-optimal solutions, i.e. solutions for which neither objective can be improved further without degrading the other objective.

For the problems of interest to this work, the initial cost function V is assumed deterministic and explicit in $\mathbf{x}$, while the loss function L is defined as a probabilistic function of an appropriate set of decision variables which are uncertain. In general, to be applicable to practical problems of interest, methods for solving Eq. (1) will have to be capable of handling both high-dimensional design variable vectors as well as high-dimensional spaces of random variables necessary for modeling the multivariate stochastic wind loads.

2.2. Performance of wind-excited systems

In this work, the loss function L is defined as a probabilistic measure of a decision variable DV, which can represent, for example, the repair cost necessary to restore the full functionality of the system under a windstorm of prescribed intensity. In particular, if *im* indicates the intensity measure of the wind event, the loss function is here expressed as:

$$L = \mathrm{E}[DV|im] + \alpha \cdot \mathrm{Std}[DV|im] \tag{2}$$

where $\mathrm{E}[DV|im]$ and $\mathrm{Std}[DV|im]$ are the expected value and the standard deviation of DV, conditional on *im*, respectively, while α is a parameter, with $\alpha \geq 0$, which can be selected according to the desired robustness of the design. In other words, α can be set to zero if the variability of the decision variable is not important, while a larger α assigns more weight to the variability, therefore resulting in a more robust design (Tootkaboni et al., 2012).

The conditional mean and standard deviation of the decision variable may be determined by solving the following integrals:

$$\mathrm{E}[DV|im] = \iiint dv \cdot p(dv|dm) \cdot p(dm|edp) \cdot p(edp|im) \cdot \mathrm{d}dv \cdot \mathrm{d}dm \cdot \mathrm{d}edp \tag{3}$$

$$\mathrm{Std}[DV|im] = \left[\iiint (dv - \mathrm{E}[DV|im])^2 \cdot p(dv|dm) \cdot p(dm|edp) \cdot p(edp|im) \cdot \mathrm{d}dv \cdot \mathrm{d}dm \cdot \mathrm{d}edp\right]^{1/2} \tag{4}$$

where $\mathrm{E}[\cdot|\cdot]$ and $\mathrm{Std}[\cdot|\cdot]$ are the operators of conditional expectation and conditional standard deviation respectively; *DM* is the damage measure indicating the damage state of the structural/nonstructural components in the system (e.g. window cracking); *EDP* is the engineering demand parameter associated with the occurrence of damage (e.g. inter-story drift ratios); and $p(\cdot|\cdot)$ indicates the conditional probability density functions. In Eqs. (3) and (4) as well as in the rest of the paper, upper-case letters will be used to indicate random variables and lower-case letters to indicate their realizations.

As will be discussed later, for the problems of interest to this work, analytical solutions to Eqs. (3) and (4) are not feasible. As a consequence, for their solution it is generally necessary to resort to stochastic simulation methods, which are generally computationally demanding, especially when finite element analyses of large-scale dynamic system are involved. The repeated evaluation of the probabilistic measure of Eq. (2), and therefore of these integrals, for different candidate designs when solving the optimization problem of Eq. (1) further exasperates the computational challenge of the problem at hand. To overcome this difficulty, an efficient bi-objective optimization method is here proposed that is based on formulating single-objective design optimization problems that can be solved efficiently through a sequential kriging-enhanced optimization approach, as will be outlined in Sec. 4. In the next section, the performance assessment framework adopted to determine the quantities appearing in Eqs. (3) and (4) for a given design $\mathbf{x}$ and intensity *im* will be presented.

3. Performance assessment

The quantities appearing in Eqs. (3) and (4) can be estimated through four separate tasks: structural and hazard analysis for the estimation of the structural response parameters of interest (*EDPs*) given an intensity *im*, damage and loss analysis for the assessment of the consequent system-level decision variables *DV*. The models that are used to carry out these tasks are discussed in the following.

3.1. Structural and hazard analysis

3.1.1. Structural response model

In this work, the engineering demand parameters, *EDPs* – i.e. the structural response parameters of interest – are defined as the non-directional absolute maximum, over a windstorm of duration T, of the structural response process $r(t)$:

$$edp(\overline{v}_H, \mathbf{u}_s) = \max_{\beta\in[0,2\pi]}\left\{\max_{t\in[0,T]}\{|r(t;\overline{v}_H,\beta,\mathbf{u}_s)|\}\right\} \tag{5}$$

where $\overline{v}_H$ is the site-specific mean wind speed at the height of the building, β denotes the wind direction, and $\mathbf{U}_s$ is a vector containing random variables used to describe the uncertainty in the structural system.

For a linear system subject to aerodynamic wind loads, the response process, $r(t)$, may be efficiently estimated through the following load-effect model (Suksuwan and Spence, 2018a):

$$\begin{aligned} r(t;\overline{v}_H,\beta,\mathbf{u}_S) &= s_1[r_B(t;\overline{v}_H,\beta) + r_R(t;\overline{v}_H,\beta,\mathbf{u}_S)] \\ &= s_1\left[\boldsymbol{\Gamma}_r^T\mathbf{f}(t;\overline{v}_H,\beta) + \boldsymbol{\Gamma}_r^T\mathbf{K}\boldsymbol{\Phi}_M\mathbf{q}_{R_M}(t;\overline{v}_H,\beta,\mathbf{u}_S)\right] \end{aligned} \tag{6}$$

where S_1 is a random variable modeling the epistemic uncertainty in using the load-effect model and is an element of $\mathbf{U}_S$; $r_B(t)$ and $r_R(t)$ are the background and resonant components of $r(t)$; $\boldsymbol{\Gamma}_r$ is a vector of influence functions, each giving the value of r due to a unit load acting at a certain degree of freedom of the system; $\mathbf{f}(t)$ is the vector of the external aerodynamic loads acting on the system; $\mathbf{K}$ is the stiffness matrix of the system; $\boldsymbol{\Phi}_M = [\phi_1,\ldots,\phi_M]$ is the mass normalized mode shape matrix considering M modes; and $\mathbf{q}_{R_M}(t) = \{q_{R_1}(t),\ldots,q_{R_M}(t)\}^T$ is a vector containing the first M resonant modal displacement response processes, which may be estimated through modal analysis.

As can be seen from Eq. (6), in this approach, M modes are considered in calculating the resonant component, while the background component is directly estimated, and is therefore not affected by modal truncation. The ith resonant modal response may be calculated as the difference between the total and the background modal displacement responses as follows:

$$q_{R_i}(t;\overline{v}_H,\beta,\mathbf{u}_S) = q_i(t;\overline{v}_H,\beta,\mathbf{u}_S) - q_{B_i}(t;\overline{v}_H,\beta,\mathbf{u}_S) \tag{7}$$

where $q_i(t)$ is the total modal response process while $q_{B_i}(t)$ is the background modal response process. To estimate, $q_i(t)$, the following equation of motion can be solved:

$$\ddot{q}_i(t) + 2s_{3_i}\zeta_i s_{2_i}\omega_i\dot{q}_i(t) + (s_{2_i}\omega_i)^2 q_i(t) = \phi_i^T\mathbf{f}(t;\overline{v}_H,\beta) \tag{8}$$

where the over-dot indicates a derivative with respect to time; ω_i and ζ_i are the modal circular frequency and damping ratio of the ith mode; S_{2_i} and S_{3_i} are random variables modeling uncertainty in ω_i and ζ_i respectively, and are elements of $\mathbf{U}_s$. The background component, $q_{B_i}(t)$, can be estimated as:

$$q_{B_i}(t;\overline{v}_H,\beta,\mathbf{u}_S) = \frac{1}{(s_{2_i}\omega_i)^2}\phi_i^T\mathbf{f}(t;\overline{v}_H,\beta) \tag{9}$$

The aerodynamic wind loads $\mathbf{f}(t)$ appearing in Eqs. (6), (8) and (9) are obtained through the stochastic wind load model presented in the following section.

3.1.2. Stochastic wind load model

The intensity measure, *IM*, of the wind event is here taken as the mean wind speed with mean recurrence interval (MRI) of y years, $\overline{v}_y$, extracted from the wind speed records at a suitable meteorological station. The purpose of this model is to relate this intensity measure $\overline{v}_y$ – which is associated with an averaging time τ, the height above ground at which measurements are taken H_{met}, and the terrain roughness length z_{01} – to the mean wind speed $\overline{v}_H$, averaged over a time period T, at the location of interest and at the height of the building H. To relate $\overline{v}_y$ and $\overline{v}_H$, a transformation of the following type can be used:

$$\overline{v}_H = \chi\left[T, H, z_0, \overline{v}_y(\tau, H_{met}, z_{01}), \mathbf{u}_E\right] \tag{10}$$

where z_0 is the roughness length at the site of interest while $\mathbf{U}_E$ is the vector containing random variables modeling uncertainties in the roughness lengths, averaging time conversion, modeling errors, sampling and observational errors in wind speed collection, and uncertainties in estimating $\overline{v}_y$. The specific transformation scheme adopted in this work can be found in Appendix C.

In order to generate realizations of the stochastic wind loads $\mathbf{f}(t)$ for a given $\overline{v}_H$ and a wind direction β, a simulation model based on the spectral proper orthogonal decomposition (POD) of wind tunnel pressure datasets (Ruan et al., 2006; Kim et al., 2018) is adopted in this work. This allows complex aerodynamic phenomena, such as vortex shedding, to be taken into account in the response estimation. Following this model, the aerodynamic wind loads $\mathbf{f}(t)$ are modeled as the superposition of N_f independent vector-valued subprocesses (Chen and Kareem, 2005; Li and Kareem, 1993; Peng et al., 2017):

$$\mathbf{f}(t;\overline{v}_H,\beta) = \sum_{j=1}^{N_f}\mathbf{f}_j(t;\overline{v}_H,\beta) \tag{11}$$

where the vector-valued subprocesses $\mathbf{f}_j(t)$ are given by:

$$\begin{aligned} \mathbf{f}_j(t;\overline{v}_H,\beta) = \sum_{l=1}^{N_l-1}\Big\{&\left|\boldsymbol{\Psi}_j(\omega_l;\beta)\right|\sqrt{2\Lambda_j(\omega_l;\overline{v}_H,\beta)\Delta\omega}\cdot\cos\big(\omega_l t + \vartheta_j(\omega_l;\beta) \\ &+ \theta_{lj}\big)\Big\} \end{aligned} \tag{12}$$

where $\Delta\omega$ is the frequency increment; $\omega_l = l\Delta\omega$ with Nyquist frequency given by $N_l\Delta\omega$; ϑ_j is a vector of complex angles whose kth component is given by $\vartheta_{jk}(\omega_l) = \tan^{-1}(\mathrm{Im}(\Psi_{jk}(\omega_l))/\mathrm{Re}(\Psi_{jk}(\omega_l)))$; θ_{lj} is an independent random variable characterizing the stochastic nature of the wind, uniformly distributed in $[0,2\pi]$; while $\Lambda_j(\omega_l)$ and $\boldsymbol{\Psi}_j(\omega_l)$ are the eigenvalues and eigenvectors of $\mathbf{f}_j(t)$. In particular, $\Lambda_j(\omega_l)$ and $\boldsymbol{\Psi}_j(\omega_l)$ can be related to the eigenvalues and eigenvectors of the scaled wind tunnel loads through the relationship:

$$\Lambda_j(\omega_l;\overline{v}_H) = \left[\left(\frac{\overline{v}_H}{\overline{v}_{ws}}\right)^2\right]^2\left(\frac{\overline{v}_{ws}}{\overline{v}_H}\right)\Lambda_j^{(ws)}(\tilde{\omega}) \tag{13}$$

$$\boldsymbol{\Psi}_j(\omega_l) = \boldsymbol{\Psi}_j^{(ws)}(\tilde{\omega}) \tag{14}$$

where $\overline{v}_{ws}$ is the mean wind speed at the top of the rigid model in the wind tunnel test; $\tilde{\omega} = (\overline{v}_{ws}/\overline{v}_H)\omega_l$; while $\Lambda_j^{(ws)}(\tilde{\omega})$ and $\boldsymbol{\Psi}_j^{(ws)}(\tilde{\omega})$ are the eigenvalues and eigenvectors of the scaled wind tunnel loads, which are obtained from solving the following eigenvalue problem:

$$\left[\mathbf{S}_{\mathbf{f}_{ws}}(\tilde{\omega};\overline{v}_{ws},\beta) - \Lambda^{(ws)}(\tilde{\omega};\overline{v}_{ws},\beta)\mathbf{I}\right]\boldsymbol{\Psi}^{(ws)}(\tilde{\omega};\beta) = 0 \tag{15}$$

where $\mathbf{S}_{\mathbf{f}_{ws}}$ is the cross power spectral density matrix of the wind load process estimated directly from the wind tunnel data collected at $\overline{v}_{ws}$. Importantly, once $\Lambda_j^{(ws)}(\tilde{\omega})$ and $\boldsymbol{\Psi}_j^{(ws)}(\tilde{\omega})$ are obtained through solving Eq. (15), they can be rapidly scaled to other wind speeds of interest through Eqs. (13) and (14). This is fundamental for the efficiency of the model, as it allows Eq. (15) to be solved only once at the wind tunnel speed $\overline{v}_{ws}$.

For convenience, all the random variables used in generating the stochastic wind loads $\mathbf{f}(t)$ are collected in the vector $\mathbf{U}_W = \{\mathbf{U}_E^T, \mathbf{U}_\theta^T\}^T$, where $\mathbf{U}_\theta$ is the vector of the random variables θ_{lj} necessary for modeling the subprocesses of Eq. (12).

3.2. Damage and loss analysis

3.2.1. Damage model

Damage to a structural or nonstructural component occurs when the demand on the component, expressed as the value assumed by a specific engineering demand parameter *EDP*, exceeds the component's capacity. In this work, all components that are susceptible to the same *EDP* are grouped into a performance group (PG). Following this approach, the total number of PGs will be indicated in the following as N_g. Given a demand value *edp*, the probability of a damage state (*DS*) occurring for each component of a PG may be determined through the corresponding fragility function, defined as:

$$\mathrm{Fr}_{DS}(edp) = \mathrm{P}(DS|edp) \tag{16}$$

In the following, the discrete variable D_{kj} is used to indicate the damage state of the *j*th component of the *k*th PG. In particular, given that N_s damage states, i.e. $[DS_1,\ldots,DS_{N_s}]$, are defined for the *j*th component of the *k*th PG, $D_{kj}=i$ if the damage state is DS_i, while $D_{kj}=0$ if no damage occurs. In general, three possible logical relationships between damage states may be assumed (Federal Emergency Management Agency (FEMA), 2012a): 1) sequential (i.e. damage states occur in sequential order); 2) mutually exclusive (i.e. occurrence of one damage state precludes another); and 3) simultaneous (i.e. two damage states can, but not necessarily, occur at the same time). Since the vast majority of damage states follow a sequential logic, it is assumed in this work. Therefore, with DS_{i+1} more severe than DS_i, each component must enter DS_i before entering DS_{i+1}. Under these circumstances, the probability that the component is in the *i*th damage state, given the demand parameter assumes the value *edp*, can be obtained from the fragility functions as:

$$\mathrm{P}\left(D_{kj}=i\middle|edp\right) = \mathrm{P}(DS_i|edp) - \mathrm{P}(DS_{i+1}|edp) = \mathrm{Fr}_{DS_i}(edp) - \mathrm{Fr}_{DS_{i+1}}(edp) \tag{17}$$

for $i=0,1,\ldots,N_s$, with $\mathrm{Fr}_{DS_0}(edp)=1$ and $\mathrm{Fr}_{DS_{N_s+1}}(edp)=0$. It should be noted that while Eq. (17) is a widely used expression, it is only exact when the fragility functions are lognormal distributions with the same dispersion.

In practice, if u_{Dkj} is a realization of a random variable uniformly distributed between 0 and 1, defined for the *j*th component of the *k*th PG, then the damage state of that component can be identified as follows:

$$d_{kj} = i \quad \text{if} \quad \mathrm{Fr}_{DS_{i+1}}(edp) < u_{Dkj} \le \mathrm{Fr}_{DS_i}(edp) \tag{18}$$

In this work, the damage states of the components are assumed as uncorrelated. Therefore, the random variables U_{Djk} are taken as independent and identically distributed. Before closing this section, it should be noted, however, that this assumption, as well as the assumption on the damage logic as sequential, is not a requirement for the optimization approach that will be presented in this work. Having said this, consideration of dependency between the damage states would significantly complicate the damage and loss models, especially if higher order moments were considered.

3.2.2. Loss model

Once the damage state of the *j*th component of the *k*th PG is known, the corresponding decision variable, dv_{kj}, can be estimated as:

$$dv_{kj} = \mathrm{F}^{-1}_{DV_{kj}}\left(u_{Lkj}\middle|d_{kj}\right) \tag{19}$$

where u_{Lkj} is a random number uniformly distributed between 0 and 1 while $F_{DV_{kj}}$ is the distribution function of DV_{kj} with $\mathrm{F}^{-1}_{DV_{kj}}(u_{Lkj}|d_{kj}=0)=0$, i.e. the decision variable is zero in absence of any damage. The distributions $F_{DV_{kj}}$ are termed consequence functions in the following.

The system-level decision variable can then be estimated as:

$$dv = \sum_{k=1}^{N_g} dv_k = \sum_{k=1}^{N_g}\sum_{j=1}^{N_c^k} w_{kj} dv_{kj} \tag{20}$$

where DV_k is the decision variable associated with the *k*th PG, N_c^k is the total number of components in the *k*th PG, while $0 \le w_{kj} \le 1$ are coefficients that take into account the economies of scale or, if DV_k is a repair time, the simultaneous or sequential nature of the repair actions. Typically, if DV_k is a repair cost, all the w_{kj} can be assumed equal to one.

3.3. System-level loss statistics

In order to estimate the second order statistics, $\mathrm{E}[DV]$ and $\mathrm{Std}[DV]$, of the system-level decision variable, DV, it is first convenient to take advantage of the linear structure of Eq. (20) and relate $\mathrm{E}[DV]$ and $\mathrm{Std}[DV]$ to the second order statistics of the decision variables associated with each PG as follows:

$$\mathrm{E}[DV] = \sum_{k=1}^{N_g} \mu_{DV_k} \tag{21}$$

$$\mathrm{Std}[DV] = \sqrt{\sum_{k=1}^{N_g}\sum_{m=1}^{N_g} \rho_{km}\sigma_{DV_k}\sigma_{DV_m}} \tag{22}$$

where μ_{DV_k} is the expected value of the decision variable associated with the *k*th PG (i.e. the expected value of the decision variable due to damage to the components of the *k*th PG); ρ_{km} is the correlation coefficient between DV_k and DV_m; while σ_{DV_k} and σ_{DV_m} are the standard deviations of DV_k and DV_m respectively. Equations (21) and (22) illustrate how the estimation of $\mathrm{E}[DV]$ and $\mathrm{Std}[DV]$ require the estimation of μ_{DV_k}, σ_{DV_k}, and ρ_{km}. Approaches to this end will be discussed below.

3.3.1. Analytical approach

The second order statistics μ_{DV_k}, σ_{DV_k} and ρ_{km} can be estimated analytically through writing them in terms of the laws of total expectation and variance as:

$$\mu_{DV_k} = \mathrm{E}\left[\mu_{DV_k|EDP_k}\right] \tag{23}$$

$$\sigma_{DV_k} = \sqrt{\mathrm{E}\left[\sigma^2_{DV_k|EDP_k}\right] + \mathrm{Var}\left[\mu_{DV_k|EDP_k}\right]} \tag{24}$$

$$\rho_{km} = \frac{\mathrm{Cov}\left[\mu_{DV_k|EDP_k}, \mu_{DV_m|EDP_m}\right]}{\sigma_{DV_k}\sigma_{DV_m}} \tag{25}$$

where $\mu_{DV_k|EDP_k}$ and $\sigma^2_{DV_k|EDP_k}$ are the conditional expected value and variance of DV_k given EDP_k, respectively; while $\mu_{DV_m|EDP_m}$ is the conditional expected value of DV_m given EDP_m. Because for the loss model of Sec. 3.2 the conditional statistics $\mu_{DV_k|EDP_k}$ and $\sigma^2_{DV_k|EDP_k}$ can be estimated through analytical functions, see (Baker and Cornell, 2008), Eqs. (23)-(25) can be solved exactly. Unfortunately, the aforementioned functions are nonlinear. This implies that the exact solution to Eqs. (23)-(25) requires the numerical resolution of the following expressions:

$$\mu_{DV_k} = \int_{-\infty}^{\infty} g_\mu^{NL}(edp_k)\cdot f_{EDP_k}(edp_k)\mathrm{d}edp_k \tag{26}$$

$$\sigma_{DV_k} = \sqrt{\int_{-\infty}^{\infty}\left[g_{\sigma^2}^{NL}(edp_k) + \left(g_\mu^{NL}(edp_k) - \mu_{DV_k}\right)^2\right]\cdot f_{EDP_k}(edp_k)\mathrm{d}edp_k} \tag{27}$$

$$\rho_{km} = \frac{\int_{-\infty}^{\infty}\int_{-\infty}^{\infty} g_{\mu}^{NL}(edp_k)\cdot g_{\mu}^{NL}(edp_m)\cdot f_{EDP_k,EDP_m}(edp_k, edp_m)\mathrm{d}edp_k\mathrm{d}edp_m - \mu_{DV_k}\mu_{DV_m}}{\sigma_{DV_k}\sigma_{DV_m}} \tag{28}$$

where g_{μ}^{NL} and $g_{\sigma^2}^{NL}$ are the nonlinear functions describing $\mu_{DV_i|EDP_i}$ and $\sigma^2_{DV_i|EDP_i}$ in terms of edp_i; f_{EDP_k} is the marginal probability density function (pdf) of EDP_k; while f_{EDP_k,EDP_m} is the joint probability density function (jpdf) between EDP_k and EDP_m.

Two fundamental difficulties arise in solving Eqs. (26)-(28). Firstly, as the number of demands parameters, EDP_k, increases, the numerical effort involved in solving Eqs. (26)-(28) quickly increases. Secondly, the marginal and joint pdfs, f_{EDP_k} and f_{EDP_k,EDP_m}, of the random vector **EDP** are not known *a priori* for the problems of interest to this work. Therefore, implementation of the analytical scheme of this section would require additional analysis (e.g. stochastic simulation) for the identification of the marginal and pair-wise joint pdfs of **EDP**.

3.3.2. Monte Carlo simulation

In alternative to the analytical approach, samples of the group-level decision variables, DV_k, can be directly simulated according to the damage and loss analysis scheme of Sec. 3.2. In particular, if all random variables introduced in the preceding sections are gathered in a vector $\mathbf{U} = \{\mathbf{U}_S^T, \mathbf{U}_W^T, \mathbf{U}_D^T, \mathbf{U}_L^T\}^T$, where $\mathbf{U}_D$ and $\mathbf{U}_L$ are vectors collecting all random variables U_{Dkj} and U_{Lkj}, respectively, the expected value and the standard deviation of a variable Q (e.g. the decision variable DV_k, or the demand parameter EDP_k), given a value of the intensity measure $\bar{v}_y$, may be estimated as:

$$\mathrm{E}\left[Q|\bar{v}_y\right] \approx \frac{1}{N_s}\sum_{i=1}^{N_s} q\left(\mathbf{u}^{(i)}, \bar{v}_y\right) \tag{29}$$

$$\mathrm{Std}\left[Q|\bar{v}_y\right] \approx \sqrt{\frac{1}{N_s-1}\sum_{i=1}^{N_s}\left(q\left(\mathbf{u}^{(i)}, \bar{v}_y\right) - \mathrm{E}\left[Q|\bar{v}_y\right]\right)^2} \tag{30}$$

where N_s is the total number of samples used in the simulation, and $\mathbf{u}^{(i)}$ is the ith realization of vector $\mathbf{U}$. Also, the correlation coefficient between any two variables Q_j and Q_k can be found from the samples as:

$$\begin{aligned}\mathrm{Rho}\left[Q_j, Q_k|\bar{v}_y\right] \approx \left(\frac{1}{\mathrm{Std}\left[Q_j|\bar{v}_y\right]\cdot\mathrm{Std}\left[Q_k|\bar{v}_y\right]}\right)\frac{1}{N_s-1}\sum_{i=1}^{N_s}\Big(q_j\left(\mathbf{u}^{(i)}, \bar{v}_y\right) \\ - \mathrm{E}\left[Q_j|\bar{v}_y\right]\Big)\left(q_k\left(\mathbf{u}^{(i)}, \bar{v}_y\right) - \mathrm{E}\left[Q_k|\bar{v}_y\right]\right)\end{aligned} \tag{31}$$

In general, for the problems of interest to this work (i.e. problems with high-dimensional vectors of dependent demands with unknown marginal and pair-wise joint pdfs), this approach is considerably more efficient than the analytical approach outlined in Sec. 3.3.1.

4. Proposed solution strategy

This section proposes a novel framework for solving the bi-objective design optimization problem of Eq. (1) with performance objectives defined in terms of the probabilistic loss measures posed in Eq. (2) calculated according to the models of Sec. 3. The framework is based on using the ε-constraint approach to reformulate the bi-objective problem as a series of single-objective problems that can then be efficiently solved through the sequential kriging-enhanced optimization strategy that will be developed in this work.

4.1. The ε-constraint formulation

By following the ε-constraint approach, the bi-objective optimization problem of Eq. (1) is reformulated by transforming the loss objective into a constraint. Under these conditions, the optimization problem takes the form:

$$\begin{array}{ll}\text{Find} & \mathbf{x} = \{x_1, \dots, x_N\}^T \\ \text{to minimize} & V(\mathbf{x}) \\ \text{subject to} & L(\mathbf{x}) = \mathrm{E}[DV(\mathbf{x})] + \alpha\mathrm{Std}[DV(\mathbf{x})] \le L_0 \\ x_n \in \mathbb{X}_n & n = 1, \dots, N\end{array} \tag{32}$$

where L_0 represents a predefined loss threshold while the constraint $L(\mathbf{x}) \le L_0$ is the ε-constraint. In Eq. (32) and in the following, conditioning on the intensity measure is dropped for simplicity of notation. It should be noted that the proposed framework is equally applicable for problems formulated as a minimization of L subject to a constraint on V. Through solving a series of ε-constraint optimization problems (which are now single-objective) for different values of L_0, i.e. for $L_0 = L_0^1, L_0^2, \dots, L_0^{N_\varepsilon}$, a set of Pareto optimal solutions $(\mathbf{x}^1, \dots, \mathbf{x}^{N_\varepsilon})$ for the bi-objective optimization problem of Eq. (1) is determined.

4.2. The decoupling strategy: overview

To efficiently solve each of the ε-constraint problems of Eq. (32), for each value of L_0, it is here proposed to formulate and solve a sequence of sub-problems for which an approximation of the loss constraint is utilized in lieu of the actual constraint. This will be accomplished in two steps. First, an approximation scheme is developed to describe the relationship between the statistics of DV appearing in the constraint (E[DV] and Std[DV]) and the statistics of the demand parameters of the various PGs (μ_{EDP_k} and σ_{EDP_k}). Then, the Auxiliary Variable Vector (AVV) strategy will be used to find a relationship between μ_{EDP_k} and σ_{EDP_k} and the design variables **x**. Since both the approximation scheme and the AVVs can be defined, as explained in the following, based on the results of a single simulation carried out in a fixed design point, only one simulation is needed for the formulation and solution of each sub-problem, hence the efficiency and scalability of the proposed approach. In order to treat the inherent approximations of the approach, a sequence of sub-problems are solved, each formulated in the solution of the previous problem, until the solutions of two successive sub-problems coincide. Because each sub-problem is exact in the point of formulation, this process ensures solutions to the original problem are found.

4.3. The approximation scheme

4.3.1. The basis of the scheme

In order to treat high-dimensional problems, the variation in the demand parameters generated by a change in the design variables **x** is modeled through the AVV approach and therefore in terms of variations in the second order statistics, μ_{EDP_k} and σ_{EDP_k}, of the demands. As discussed in Sec. 3.3.1, because the relationship between the decision variables and the demand parameters is nonlinear, any variation in μ_{EDP_k} and σ_{EDP_k} cannot be directly mapped to the changes in the second order statistics of the decision variables. To overcome this, a scheme is here introduced for approximately modeling how the demand samples obtained from a Monte Carlo simulation carried out in $\tilde{\mathbf{x}}$ change as μ_{EDP_k} and σ_{EDP_k} vary due to a change in the design vector. This enables E[DV_k] and Std[DV_k] of each PG to be approximately estimated through the stochastic simulation model of Sec. 3.3.2.

With this in mind, consider a set of samples $\{edp_k^1, \dots, edp_k^{N_s}\}$, evaluated in $\tilde{\mathbf{x}}$, with associated mean and standard deviation of $\mu_{EDP_k}(\tilde{\mathbf{x}})$ and $\sigma_{EDP_k}(\tilde{\mathbf{x}})$. As the design point changes from $\tilde{\mathbf{x}}$ to $\mathbf{x}$, a set of adjusted samples $\{\overline{edp}_k^1,\ldots,\overline{edp}_k^{N_s}\}$, whose mean and standard deviation have been updated to $\mu_{EDP_k}(\mathbf{x})$ and $\sigma_{EDP_k}(\mathbf{x})$, can be conveniently generated by transforming the samples obtained in $\tilde{\mathbf{x}}$ as follows:

$$\overline{edp}_k^i(\mathbf{x}) = \frac{\sigma_{EDP_k}(\mathbf{x})}{\sigma_{EDP_k}(\tilde{\mathbf{x}})}\left(edp_k^i(\tilde{\mathbf{x}}) - \mu_{EDP_k}(\tilde{\mathbf{x}})\right) + \mu_{EDP_k}(\mathbf{x}) \qquad i = 1,\ldots,N_s \tag{33}$$

The validity of the transformation of Eq. (33) can be traced back to how, for the problems of interest to this work, the reduced variate $g_k^i = \left(edp_k^i - \mu_{EDP_k}\right)\Big/\sigma_{EDP_k}$ can be considered independent of the design variables $\mathbf{x}$ (e.g. Suksuwan and Spence, 2018b). Because the transformation of Eq. (33) is invariant with respect to this reduced variate, i.e. $\overline{g}_k^i = g_k^i$, Eq. (33) provides an accurate means to generate a sample set of demands that is consistent with changes in μ_{EDP_k} and σ_{EDP_k} generated by a change in $\mathbf{x}$ and modeled through the AVV approach. From the adjusted set of demand samples $\{\overline{edp}_k^1,\ldots,\overline{edp}_k^{N_s}\}$, the corresponding second order PG statistics μ_{DV_k}, σ_{DV_k} and ρ_{km} can be estimated through the Monte Carlo scheme of Sec. 3.3.2, from which E[DV] and Std[DV] of the system-level constraint of Eq. (32) can then be evaluated through Eqs. (21)-(22).

While the transformation of Eq. (33) enables the use of the AVV approach, and therefore eliminates the need to propagate uncertainty through the large-scale and dynamic finite element models characterizing the structural system, the evaluation of the E[DV] and Std[DV] still requires the implementation of the Monte Carlo scheme of Sec. 3.3.2 for each change in the design variable vector $\mathbf{x}$. Because in general optimization algorithms require hundreds, if not thousands, of calls to the objective/constraint functions during the optimization process, this can lead to significant computational slowdowns during the optimization process.

4.3.2. The metamodels

To enhance the computational efficiency of the approximation scheme, it is here proposed to fully decouple the approximation from the Monte Carlo scheme of Sec. 3.3.2 through the use of kriging metamodels. This will provide a deterministic mapping between the second order statistics of group-level decision variables (μ_{DV_k} and σ_{DV_k}) and the second order statistics of demand parameters (μ_{EDP_k} and σ_{EDP_k}). Because kriging metamodels are extremely cheap to evaluate, this approach can significantly speed up the internal iterations of the optimization algorithm (e.g. by two orders of magnitude for the optimality criteria algorithm of the case study of Sec. 5) as compared to the direct implementation of the approximation scheme.

From Eqs. (21) and (22), it can be seen that in order to develop a deterministic mapping between E[DV] and Std[DV] and the second order statistics of the demands, metamodels that relate μ_{DV_k} and σ_{DV_k} to μ_{EDP_k} and σ_{EDP_k}, as well as ρ_{km} to μ_{EDP_k}, σ_{EDP_k}, μ_{EDP_m} and σ_{EDP_m}, are required. However, if it is assumed that ρ_{km} is only weakly dependent on the design variables $\mathbf{x}$, then only the first set of metamodels are needed. The general validity of assuming ρ_{km} only weakly dependent on $\mathbf{x}$ can be understood by recognizing how the design variables are independent of the statistical properties of the basic random variables. Therefore, a change in design variables cannot significantly alter the statistical dependency between the decision variables of the PGs. Given their versatility, ordinary kriging metamodels (Sack et al., 1989; Forrester Keaneet al., 2008) are adopted in this work for developing the deterministic mapping. Before continuing, it should be observed that the metamodels developed in this section are approximate as they are built in terms of the approximation scheme of Sec. 4.3.1. However, construction of exact metamodels is not possible as it would require the knowledge of the marginal distributions of the demand vector **EDP** which, as discussed in Sec. 3.3.1, are not known *a priori*.

Sampling plan and calibration points. In order to calibrate the kriging metamodels $\widehat{\mu}_{DV_k}(\mu_{EDP_k},\sigma_{EDP_k})$ and $\widehat{\sigma}_{DV_k}(\mu_{EDP_k},\sigma_{EDP_k})$, N_p of observations of μ_{DV_k} and σ_{DV_k} are required at a series of points (support points) of coordinates $(\mu_{EDP_k}^{(1)}(\mathbf{x}),\sigma_{EDP_k}^{(1)}(\mathbf{x})),\ldots,(\mu_{EDP_k}^{(N_p)}(\mathbf{x}),\sigma_{EDP_k}^{(N_p)}(\mathbf{x}))$. The observations corresponding to the pth support point are indicated in the following as $\mu_{DV_k}^{(p)} = \mu_{DV_k}(\mu_{EDP_k}^{(p)},\sigma_{EDP_k}^{(p)})$ and $\sigma_{DV_k}^{(p)} = \sigma_{DV_k}(\mu_{EDP_k}^{(p)},\sigma_{EDP_k}^{(p)})$.

By carrying out a Monte Carlo simulation in the design point $\tilde{\mathbf{x}}$ through the algorithm of Sec. 3, $\mu_{EDP_k}(\tilde{\mathbf{x}})$, $\sigma_{EDP_k}(\tilde{\mathbf{x}})$ as well as $\mu_{DV_k}(\tilde{\mathbf{x}})$, $\sigma_{DV_k}(\tilde{\mathbf{x}})$ may be directly estimated from Eqs. (29) and (30). The point of coordinates $(\mu_{EDP_k}(\tilde{\mathbf{x}}),\sigma_{EDP_k}(\tilde{\mathbf{x}}))$ can therefore be chosen as the first support point of the metamodels, for which the corresponding observations are $\mu_{DV_k}^{(1)}(\tilde{\mathbf{x}})$ (for the metamodel $\widehat{\mu}_{DV_k}$), and $\sigma_{DV_k}^{(1)}(\tilde{\mathbf{x}})$ (for the metamodel $\widehat{\sigma}_{DV_k}$). The coordinates $(\mu_{EDP_k}^{(p)}(\tilde{\mathbf{x}}),\ \sigma_{EDP_k}^{(p)}(\tilde{\mathbf{x}}))$, for $p = 2,\ \ldots,\ N_p$, of the remaining $(N_p - 1)$ support points are then generated over a domain centered around this first support point through optimal Latin hypercube sampling (Morris and Mitchell, 1995). To obtain the corresponding observations of $\mu_{DV_k}^{(p)}$ and $\sigma_{DV_k}^{(p)}$ for $p = 2,\ \ldots,\ N_p$, the simulation-based approximation scheme of Sec. 4.3.1 can be invoked. The N_p observations are then collected in the vectors $\overline{\boldsymbol{\mu}}_{DV_k} = \{\mu_{DV_k}^{(1)},\ldots,\mu_{DV_k}^{(N_p)}\}^T$ and $\overline{\boldsymbol{\sigma}}_{DV_k} = \{\sigma_{DV_k}^{(1)},\ldots,\sigma_{DV_k}^{(N_p)}\}^T$ which will be used, as explained in the following, for the calibration of the two kriging metamodels $\widehat{\mu}_{DV_k}$ and $\widehat{\sigma}_{DV_k}$.

Kriging prediction model. In this section, since the kriging model formulation is the same for $\widehat{\mu}_{DV_k}$ and $\widehat{\sigma}_{DV_k}$, the symbol y will be used to indicate either μ_{DV_k} or σ_{DV_k} so to avoid unnecessary repetition. Given a set of observations at the points of the sampling plan, $\overline{\mathbf{y}}$, a kriging prediction of the function $y(\mu_{EDP_k},\sigma_{EDP_k})$ is given by:

$$\widehat{y}(\mu_{EDP_k},\sigma_{EDP_k}) = \widehat{m} + \boldsymbol{\Omega}^T(\mu_{EDP_k},\sigma_{EDP_k})\mathbf{R}^{-1}\left(\overline{\mathbf{y}} - \mathbf{1}\widehat{m}\right) \tag{34}$$

where $\widehat{y}$ represents the kriging prediction of y; $\widehat{m}$ is the maximum likelihood estimator of the mean of the random field defined by taking $\overline{\mathbf{y}}$ as a realization of a Gaussian process; $\boldsymbol{\Omega}$ is an $N_p\times 1$ vector collecting the basis functions that depend on μ_{EDP_k} and σ_{EDP_k}; and $\mathbf{R}^{-1}(\overline{\mathbf{y}} - 1\widehat{m})$ are the weights assigned to the basis functions with $\mathbf{1}$ denoting the $N_p\times 1$ unit vector. In particular, in defining $\boldsymbol{\Omega}$ and $\mathbf{R}$, a square exponential function is here assumed for the correlation function, as:

$$\begin{aligned}&\mathrm{Corr}\left[y\left(\mu_{EDP_k}^{(i)},\sigma_{EDP_k}^{(i)}\right),y\left(\mu_{EDP_k}^{(j)},\sigma_{EDP_k}^{(j)}\right)\right]\\&\quad=\exp\left[-\left(\theta_\mu\left|\mu_{EDP_k}^{(i)}-\mu_{EDP_k}^{(j)}\right|^2+\theta_\sigma\left|\sigma_{EDP_k}^{(i)}-\sigma_{EDP_k}^{(j)}\right|^2\right)\right]\end{aligned} \tag{35}$$

where θ_μ and θ_σ are the parameters of the kriging metamodel. Based on the correlation functions of Eq. (35), the ith basis function is derived as:

$$\Omega_i(\mu_{EDP_k},\sigma_{EDP_k}) = \mathrm{Corr}\left[y\left(\mu_{EDP_k}^{(i)},\sigma_{EDP_k}^{(i)}\right),y\left(\mu_{EDP_k},\sigma_{EDP_k}\right)\right] \tag{36}$$

while the element of the ith row and jth column of $\mathbf{R}$ is given by:

$$R_{ij} = \mathrm{Corr}\left[y\left(\mu_{EDP_k}^{(i)},\sigma_{EDP_k}^{(i)}\right),y\left(\mu_{EDP_k}^{(j)},\sigma_{EDP_k}^{(j)}\right)\right] \tag{37}$$

Having defined $\mathbf{R}$, $\widehat{m}$ may be obtained from the following expression:

$$\widehat{m} = \frac{\mathbf{1}^T\mathbf{R}^{-1}\overline{\mathbf{y}}}{\mathbf{1}^T\mathbf{R}^{-1}\mathbf{1}} \tag{38}$$

4.4. The auxiliary variable vectors

The approximation scheme Sec. 4.3 provides a means to relate changes in the second order statistics of the decision variables associated with each PG with changes in the second order statistics of the demand parameters, i.e. μ_{EDP_k} and σ_{EDP_k}. As already mentioned, in order to relate these last to changes in the design variables $\mathbf{x}$, the concept of auxiliary variable vectors (AVVs) (Spence et al., 2016) is leveraged in this work.

To this end, consider a design point $\tilde{\mathbf{x}}$ in which the Monte Carlo scheme of Sec. 3.3.2 has been carried out with the aim of evaluating the performance of the system in $\tilde{\mathbf{x}}$. Through the augmentation of the simulation process reported in Appendix A, the AVVs, indicated as $\widehat{\boldsymbol{\Upsilon}}_k(\tilde{\mathbf{x}})$ and $\check{\boldsymbol{\Upsilon}}_k(\tilde{\mathbf{x}})$, can be defined in $\tilde{\mathbf{x}}$ for each PG. The interest in defining the AVVs lies in how it has been shown that they are insensitive to any changes of the design variables around $\tilde{\mathbf{x}}$ (e.g. Spence et al., 2016; Bobby et al., 2017). This fundamental property allows the following approximate relationships to be introduced for estimating μ_{EDP_k} and σ_{EDP_k} for a point $\mathbf{x}$ that differs from $\tilde{\mathbf{x}}$:

$$\mu_{EDP_k}(\mathbf{x}) \approx \widehat{\mu}_{EDP_k}(\mathbf{x}) = \boldsymbol{\Gamma}_{r_k}^T(\mathbf{x})\widehat{\boldsymbol{\Upsilon}}_k(\tilde{\mathbf{x}}) \tag{39}$$

$$\sigma_{EDP_k}(\mathbf{x}) \approx \widehat{\sigma}_{EDP_k}(\mathbf{x}) = \boldsymbol{\Gamma}_{r_k}^T(\mathbf{x})\check{\boldsymbol{\Upsilon}}_k(\tilde{\mathbf{x}}) \tag{40}$$

where $\boldsymbol{\Gamma}_{r_k}$ is the vector of influence functions whose ith component gives the response in EDP_k due to a unit load applied at the ith degree of freedom of the system, i.e. the influence functions of the load effect model of Eq. (6).

4.5. Formulation and solution of the sub-problem

Once a full Monte Carlo simulation is carried out in the current design point $\tilde{\mathbf{x}}$, the decoupled approximation scheme can be constructed as outlined in Sec. 4.3.2 and the AVVs can be defined to obtain the relationships illustrated in Sec. 4.4. This allows the following ε-constraint optimization sub-problem to be formulated:

$$\begin{aligned}
&\text{Find} \quad \mathbf{x} = \{x_1, \ldots, x_N\}^T \\
&\text{to minimize} \quad V(\mathbf{x}) \\
&\text{subject to} \quad \widehat{L}(\mathbf{x}) = \sum_{k=1}^{N_g} \widehat{\mu}_{DV_k}\left(\widehat{\mu}_{EDP_k}(\mathbf{x}), \widehat{\sigma}_{EDP_k}(\mathbf{x})\right) \\
&+\alpha\left[\sum_{k=1}^{N_g}\sum_{m=1}^{N_g} \tilde{\rho}_{km}\widehat{\sigma}_{DV_k}\left(\widehat{\mu}_{EDP_k}(\mathbf{x}), \widehat{\sigma}_{EDP_k}(\mathbf{x})\right)\cdot\widehat{\sigma}_{DV_m}\left(\widehat{\mu}_{EDP_m}(\mathbf{x}), \widehat{\sigma}_{EDP_m}(\mathbf{x})\right)\right]^{1/2} \le L_0 \\
&x_n \in \mathbb{X}_n \quad n = 1, \ldots, N
\end{aligned} \tag{41}$$

where $\tilde{\rho}_{km}$ is the correlation coefficient between DV_k and DV_m evaluated in $\tilde{\mathbf{x}}$.

Due to the explicit and computationally cheap nature of the ε-constraint in this problem formulation, any gradient/non-gradient optimization algorithm can be used for its solution. In particular, in this work, the pseudo-discrete optimality criteria (OC) algorithm (Chan et al., 1995) is adopted. The derivation of the sensitivities necessary for the implementation of the algorithm is reported in Appendix B.

For implementation purposes within the algorithm illustrated in the following section, besides the occurrence of convergence, if, during the search for the optimal point, the OC algorithm considers a candidate point $\mathbf{x}$ whose corresponding values of μ_{EDP} and σ_{EDP} are at the edge of the domain of the metamodels, the algorithm is terminated and the last candidate point is used as output.

4.5.1. Adaptive sequential optimization algorithm

The solution of the optimization sub-problem of Eq. (41) will in general be affected by the approximations that were introduced in the formulation of the ε-constraint, i.e. by the fact that the sub-problem is exact only in the design point in which both the approximation scheme and the AVVs are derived. Hence, the optimal point found will in general be different from the optimal point of the original ε-constraint problem of Eq. (32). To obtain an exact solution to the original ε-constraint problem, sequential optimization strategies have been seen to be effective (e.g. Du and Chen, 2004; Schuëller and Jensen, 2008). Therefore, in this work, a sequential optimization algorithm is developed, consisting in solving a series of sub-problems, of the kind outlined in Eq. (41), each formulated in the solution of the previous sub-problem, until convergence is reached, i.e. until the solution points of two consecutive design cycles coincide, within a set tolerance. Each formulation and solution of a sub-problem is termed a design cycle (DC). At convergence, since both the approximation scheme and the AVVs are exact in the point where the sub-problem is formulated, the ε-constraint – and therefore the solution – is not affected by any approximations. In addition, at each design cycle, an adaptive strategy is adopted for formulating the approximation scheme, which takes advantage of the information gathered in the previous design cycle about the most promising region of the search space. This adaptivity results in a more accurate prediction in the region around the current design point and ultimately in a faster convergence.

The proposed adaptive sequential optimization algorithm can be summarized as follows:

1. Initialization: set $\mathrm{DC} = 1$ and $\tilde{\mathbf{x}} = \mathbf{x}_0$ with $\mathbf{x}_0$ denoting the initial design; generate an optimal sampling plan with N_p points, including the central point. The sampling plan is indicated as a set of points $\mathbf{H} = \{(z_1^{(1)}, z_2^{(1)}), \ldots, (z_1^{(N_p)}, z_2^{(N_p)})\}$, where (z_1, z_2) are normalized coordinates.
2. Run a Monte Carlo simulation in $\tilde{\mathbf{x}}$ and calculate the first (central) support point of the metamodels $(\mu_{EDP_k}^{(1)}(\tilde{\mathbf{x}}), \sigma_{EDP_k}^{(1)}(\tilde{\mathbf{x}}))$, for each PG, i.e. $k = 1, \ldots, N_g$.
3. Set the limits of the search domain as $[(1-\delta_\mu)\mu_{EDP_k}^{(1)}, (1+\delta_\mu)\mu_{EDP_k}^{(1)}] \times [(1-\delta_\sigma)\sigma_{EDP_k}^{(1)}, (1+\delta_\sigma)\sigma_{EDP_k}^{(1)}]$, where δ_μ and δ_σ are assumed equal to 0.8 for the first DC and 0.5 for the following DCs. Scale the normalized sampling plan $\mathbf{H}$ to the adaptive search domain in the space of μ_{EDP_k} and σ_{EDP_k} centered at $(\mu_{EDP_k}^{(1)}(\tilde{\mathbf{x}}), \sigma_{EDP_k}^{(1)}(\tilde{\mathbf{x}}))$.
4. Determine the calibration points of the metamodels, $\overline{\boldsymbol{\mu}}_{DV_k}$ and $\overline{\boldsymbol{\sigma}}_{DV_k}$ (Sec. 4.3.2). Construct the kriging metamodels (Sec. 4.3.2), calculate the AVVs (Sec. 4.4) and formulate the sub-problem in $\tilde{\mathbf{x}}$ of Eq. (41).
5. Solve the sub-problem until convergence or termination, therefore defining $\mathbf{x}^{(DC)}$ (optimal point, in case of convergence, or last point, in case of termination) and $V^{(DC)} = V(\mathbf{x}^{(DC)})$.
6. Check for convergence: if $|V^{(DC)} - V^{(DC-1)}| < \delta_1 V^{(DC-1)}$, end optimization with $\mathbf{x}^{(DC)}$ as the final design; otherwise, set $\tilde{\mathbf{x}} = \mathbf{x}^{(DC)}$, $DC = DC + 1$, and return to Step 2.

In order to increase the efficiency of the algorithm, if, when returning to Step 2 at the end of a given DC, the change in $\mu_{EDP_k}^{(1)}(\tilde{\mathbf{x}})$ and the change in $\sigma_{EDP_k}^{(1)}(\tilde{\mathbf{x}})$, for $k = 1, \ldots, N_g$, are less than a value δ_2 with respect to the same quantities at the previous DC, then only the central point of the sampling plan, i.e. the point of coordinates $(\mu_{EDP_k}^{(1)}(\tilde{\mathbf{x}}), \sigma_{EDP_k}^{(1)}(\tilde{\mathbf{x}}))$, is updated in Step 4 (Step 3 is therefore unnecessary). This eliminates the need to evaluate μ_{DV_k} and σ_{DV_k} at other support points and therefore results in an increased efficiency.

5. Application

The example presented in this section illustrates how the proposed bi-objective optimization approach can be efficiently applied to a large-scale structural system to find optimal designs that minimize the material volume of the structural system and the system-level wind-induced total losses, under a wind with a 1700-year MRI. In particular, the total losses are expressed in terms of a DV which is assumed to be the total repair cost. Since the cladding system plays a fundamental role in defining the performance of wind-excited systems, total losses associated with damage to this system due to excessive structural response will be considered as the DV.

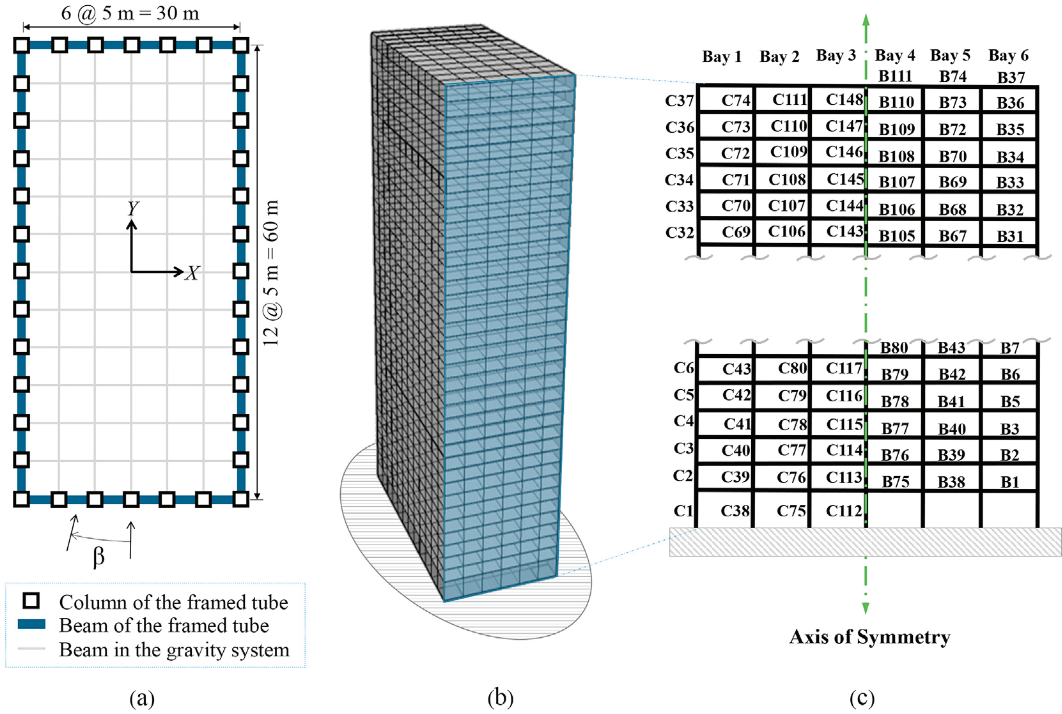

Fig. 1. Layout of the example structure: (a) plan view; (b) 3D view; (c) beam and column group assignments for one of the X-direction moment-resisting frames.

5.1. Structural model

The large-scale structural system, shown in Fig. 1, consists in a 37-story rectangular building. The first story height is 6 m while the other stories are 4 m high, resulting in a total height of 150 m. The total width and total depth of the system are 30 m and 60 m, respectively. In this example, one of the two identical X-direction lateral load-resisting frames of the 3-dimensional steel tube system is to be designed. The beams and columns of the X-direction load-resisting frames are grouped symmetrically with respect to the vertical central line as shown in Fig. 1(c). All beams are chosen to belong to the family of AISC (American Institute of Steel Construction) W24 steel profiles (i.e. a complete list from W24 $\times$ 55 to W24 $\times$ 492 is considered). All columns are square box sections defined by mid-line diameters, b_i, that must belong to the discrete set {0.20 m, 0.21 m, …, 3.99 m, 4.00 m}, while the wall thickness is given by $b_i/20$. This grouping scheme results in a total of 259 design variables. In the initial design, the profile W24 $\times$ 176 is assigned to all beams, while a mid-line diameter of 0.60 m is used for all the columns. The floor systems are assumed to be rigid diaphragms with area density of 0.1 t/m^2. In estimating the resonant response, the first three modes were considered, with the mean circular frequencies of the initial design being $\omega_1 = 1.02$ rad/s, $\omega_2 = 3.25$ rad/s, and $\omega_3 = 6.02$ rad/s. The mean modal damping ratios were taken as 1.5%. The distributions of the uncertain parameters of the vector $\mathbf{U}_s$ associated with the response estimation (Eqs. (6), (8) and (9)) are reported in Table 1.

5.2. Hazard and wind model description

The building is assumed to be located in the Miami area of Florida, USA. In modeling the hurricane wind hazard, the dataset of milepost 1450 (i.e. Miami) of the hurricane database provided by the National Institute of Standards and Technology (NIST) was considered (National Institute of Standards and Technology, 2016). The wind speeds of the dataset were obtained with an averaging time $\tau = 60$ s, roughness length $z_{01} = 0.05$ m, and height at meteorological station $H_{met} = 10$ m. In transforming samples of $\overline{v}_y$ into samples of wind speeds at the site of interest, $\overline{v}_H$, the transformation scheme provided in Appendix C was used, with averaging time $T = 3600$ s, roughness length at the site of interest $z_0 = 2$ m, and distribution of the random parameters reported in Table C.3. In calibrating the data-driven stochastic wind load model of Sec. 3.1.2, datasets of synchronously measured pressures obtained from the Wind Pressure Database of the Tokyo Polytechnic University (TPU) (Tokyo Polytechnic University, 2008) were utilized. In this example, the datasets corresponding to wind blowing down the X and Y directions (i.e. alongwind and acrosswind actions) were considered. The wind tunnel tests were carried out on a 1:300 scale model with a mean wind speed at the top of the rigid model of 11 m/s. A total number of 510 pressure taps were used, with a signal length of 32 s with sampling frequency of 1000 Hz. In calculating the wind loads acting on each frame, 1/2 of the X-direction load was considered for each wind direction, while the first six POD spectral modes of the integrated and scaled loads were considered in this example.

Table 1
Marginal distributions for the components of the vector $\mathbf{U}_S$.

Variable	Mean	C.O.V.	Distribution	Ref.
S_1	1	0.025	Trunc. Normal	Minciarelli et al. (2001)
$S_{2_i}*$	1	0.3	Lognormal	Bashor et al. (2005)
$S_{3_i}*$	1	0.01	Lognormal	Bashor et al. (2005)

* for.$i = 1, \ldots, M$

5.3. Loss model

A midrise stick-built curtain wall is considered forming the building envelope. Cladding components are susceptible to damage due to inter-story drift, therefore the maximum inter-story drift ratio in the plane of the panel is assumed as EDP_k. As a result, all cladding components of the same floor are grouped in the same PG, for a total of 37 PGs each consisting of 60 components. Three sequential damage states are defined for all components; the suite of fragility curves with associated consequence functions were obtained from the fragility database of FEMA (Federal Emergency Management Agency (FEMA), 2012b) and are reported here for convenience in Table 2.

Table 2
Parameters of the fragility and consequence functions in terms of repair cost. All fragility functions are lognormal.

DS	Description	Fragility Functions		Repair Cost	
		μ_f	β_f	μ_c [$]	β_c
1	Gasket seal failure	0.0260	0.25	2055	0.1668
2	Glass cracking	0.0268	0.25	2364	0.1185
3	Glass falling out	0.0339	0.25	2955	0.1185

5.4. Optimization

The values of the limit L_0 used in the ε-constraint formulation of Eq. (32) were set to \$100000, \$250000, \$400000, \$700000, \$1000000. Various levels of robustness were investigated by varying the value of parameter α ($\alpha = 0, 1, 2$). A number $N_s = 8000$ of samples were used in the Monte Carlo simulation. In implementing the proposed optimization framework, δ_1 was set to 10^{-6} and δ_2 was set to 0.02. The discrete optimization scheme outlined in (Chan et al., 1995) was adopted for solving the sub-problems, due to the discrete nature of the design variables.

5.5. Results and discussion

Fig. 2 shows sets of Pareto optimal points, in the space of the two objectives V and L, associated with different levels of robustness (i.e. values of α). Since three values of α have been considered, and the ε-constraint optimization was run for five values of ε, a total of 15 designs were obtained. As expected, for a given value of α, the probabilistic loss measure under a wind with MRI of 1700 years is higher for a lower initial cost (i.e. less material volume), while, given a certain loss measure, a higher initial cost (i.e. a heavier system) is required if a higher value of α (i.e. a more robust structure) is chosen.

It can be observed that α is directly related to the probability of exceeding any given loss threshold L_0. Indeed, an increase in α corresponds to reducing the overall response of the system, and therefore the probability of exceeding any given L_0. To estimate this probability for a given value of α and L_0, the N_s samples of the final Monte Carlo simulation carried out in solving the optimization problem of Eq. (32) through the proposed algorithm of Sec. 4.5.1 can be used to evaluate the following expression:

$$\mathrm{P}(DV > L_0|\overline{v}_{1700}) = \frac{1}{N_s}\sum_{i=1}^{N_s} I_i\left(\mathbf{u}^{(i)}, \overline{v}_{1700}\right) \quad (42)$$

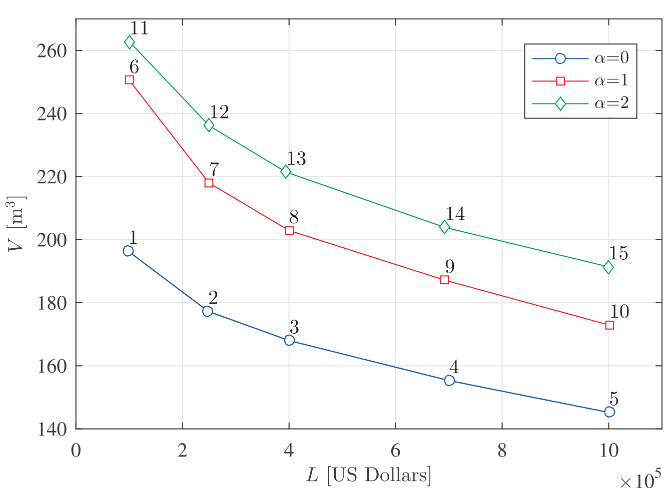

Fig. 2. Pareto fronts of optimal points in the space of the objective functions for different values of the parameter α.

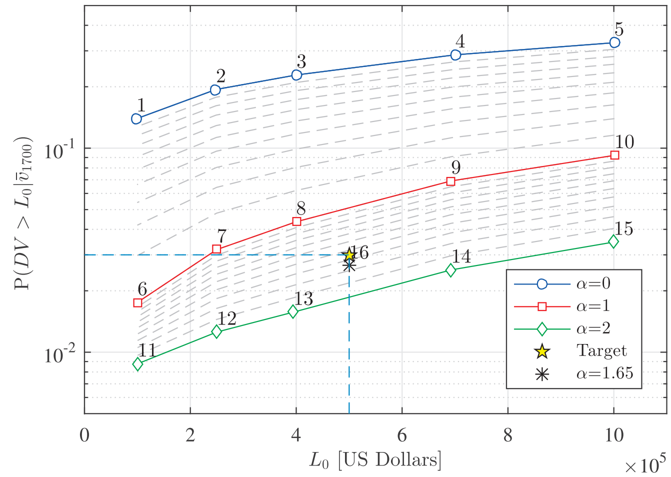

Fig. 3. Probability of exceedance of the loss threshold L_0 for various Pareto-optimal designs. Target point with $\mathrm{P}(DV > \$500000|\overline{v}_{1700}) = 0.03$ and point obtained by running simulation #16, with $\alpha = 1.65$, are also shown.

where I_i is an indicator function that assumes the value 1 if $dv(\mathbf{u}^{(i)}, \overline{v}_{1700}) \geq L_0$ and 0 otherwise. By evaluating Eq. (42) for each of the 15 Pareto-optimal configurations of Fig. 2, the system-level failure probabilities shown in Fig. 3 are obtained. The practical significance of Fig. 3 is that not only does it provide a more complete picture of the system's performance, it also provides a means for decision-makers to identify which value of α to consider in choosing an optimal trade-off solution. For example, if the stakeholders' performance objective of interest is to achieve designs with less than a 3% probability of exceeding \$500000 of repair cost for a 1700-year MRI windstorm, then, from the linearly interpolated dotted lines of Fig. 3, a value of approximately $\alpha = 1.65$ should be considered. Once the value of α is identified, an additional constrained optimization with $\alpha = 1.65$ and $L_0 = \$500000$ can be run to check the effective failure probability and to identify the set of design variables defining the optimal trade-off solution. For this example, this corresponds to design #16, which, as indicated in Fig. 3, has a failure probability of 2.63%. This examples illustrates how Figs. 2 and 3 provide an effective and concise system-level decision space for identifying optimal trade-off solutions. It should be observed that the accuracy of the interpolated results can be increased as desired by increasing the number of loss thresholds considered in the ε-constraint problem as well as the number of steps in the range considered for α.

5.5.1. Numerical performance of the ε-constraint solution strategy

To illustrate the performance of the sequential optimization algorithm of Sec. 4.5.1, Figs. 4 and 5 show the convergence histories of the two objective functions, material volume and loss respectively, for design #9. The efficiency of the proposed method is apparent from the limited number of design cycles required to obtain convergence. Indeed, it can be seen that a design that satisfies the constraint was obtained after only three design cycles, with the remaining design cycles fine-tuning the objective function of the ε-constraint problem. Fig. 5 shows the comparison between the approximate and exact loss values at the end of each design cycle. As can been seen, notwithstanding the significant changes in loss in the first couple of design cycles, the approximation scheme introduced in this work proved effective with rapid and steady convergence to the exact value. Similar results were seen for all 16 of the design points of Figs. 2 and 3.

To illustrate the adaptive updating of the kriging metamodels during the optimization process, Figs. 6 and 7 report the kriging models constructed for μ_{DV_k} and σ_{DV_k} during the resolution of the ε-constraint problem associated with design #9 and performance group $k = 22$. The largest kriging surfaces of Figs. 6 and 7 correspond to the first design

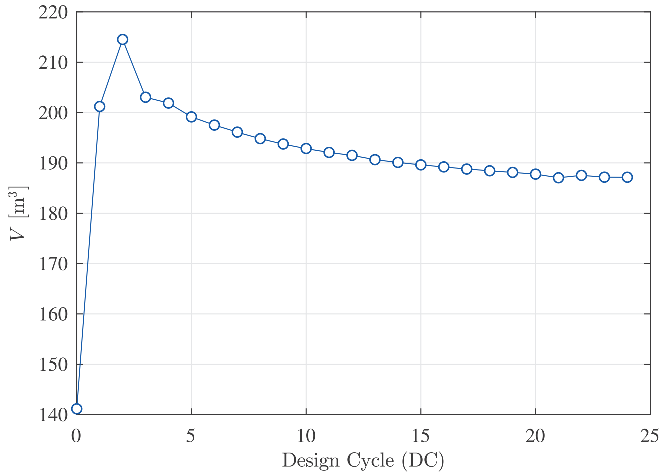

Fig. 4. Convergence history of the objective function V for design #9.

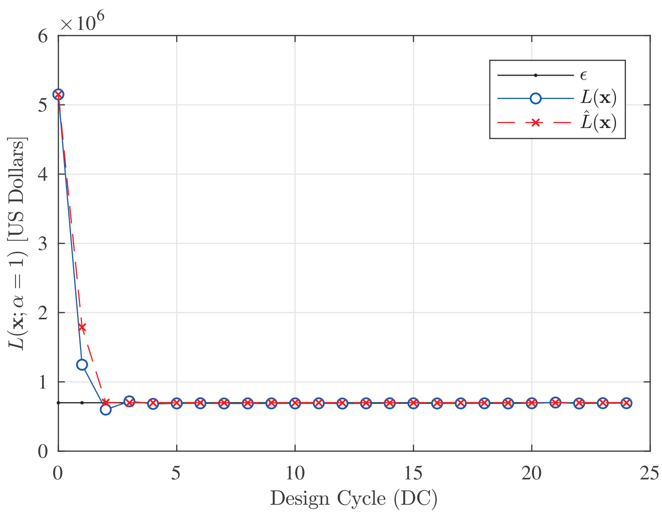

Fig. 5. Convergence history of the objective function L for design #9 ($\alpha = 1$, $\varepsilon = \$700000$). The approximate value of L, $\widehat{L}$, is also shown.

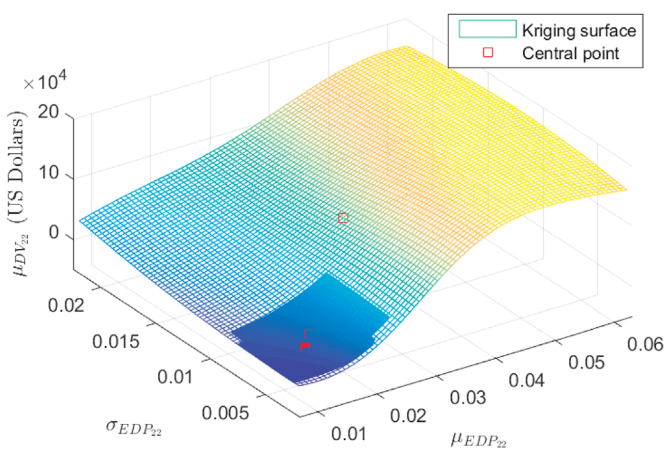

Fig. 6. Example of adaptively updated kriging metamodel of $\mu_{DV_{22}}$ for design #9.

cycle and allow a global search of the design space, while the smaller surfaces correspond to the updating scheme that adaptively concentrates the solution efforts to the region around which the first candidate solution was identified. The overall quality of the initial kriging models can

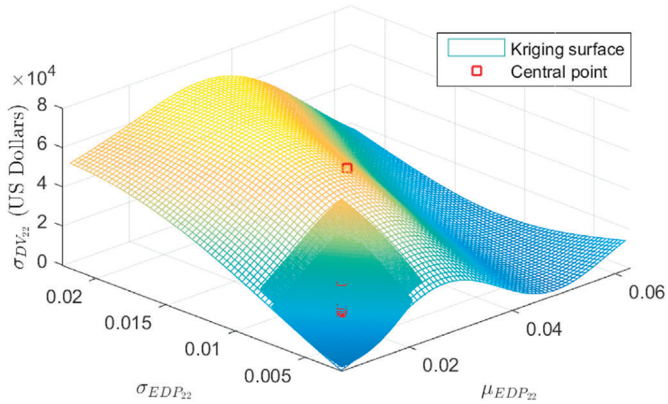

Fig. 7. Example of adaptively updated kriging metamodel of $\sigma_{DV_{22}}$ for design #9.

be clearly seen from the strong correspondence between the kriging models constructed in design cycles successive to the first. Similar results were seen for all PGs.

Finally, it should be observed that from a theoretical standpoint, the proposed approach could treat multiple probabilistic objectives. Indeed, the approximation scheme of Sec. 4.3 and the AVVs of Sec. 4.4 can be simultaneously applied to more than one probabilistic objective. Because, after approximation, both the objective and constraint functions are deterministic from the perspective of the sub-problem of Eq. (41), the sequential solution strategy of Sec. 4.5.1 would (after appropriate notation changes) be equally applicable. Therefore, as long as the probabilistic objective can be described through loss and damage models of the type outlined in this work, there is no theoretical reason that the approach could not be applied to problems involving two probabilistic objectives.

Before closing this section, it should also be observed that, while this work was based on using kriging metamodels for defining the functions $\mu_{DV_k}(\mu_{EDP_k}, \sigma_{EDP_k})$ and $\sigma_{DV_k}(\mu_{EDP_k}, \sigma_{EDP_k})$ (i.e. the functions between the second order moments of the group losses and the second order moments of the group demands), alternative approaches could be considered. In particular, future developments of this work will focus on defining new mappings that seek to take advantage of the analytic expressions that can be derived for the conditional moments $\mu_{DV_k|EDP_k}$ and $\sigma_{DV_k|EDP_k}$.

6. Conclusions

This paper presented an efficient bi-objective design optimization framework for uncertain wind-excited systems. Two competing objectives were considered: the material volume of the structure, which is associated to the initial cost, and a system-level probabilistic measure of the anticipated wind-induced losses of the system under wind events of prescribed intensities. The challenge in defining such a framework lies in the necessity of using stochastic simulation-based performance assessment frameworks within a bi-objective optimization written in terms of high-dimensional vectors of design variables. To overcome this challenge, a framework is proposed based on reformulating the original problem into a series of single-objective problems through the ε-constraint approach. To efficiently solve each ε-constraint problem, a sequential kriging-enhanced optimization scheme is introduced that is based on decoupling the probabilistic performance assessment from the optimization problem. This is achieved through the introduction of a high-quality optimization sub-problem that is defined in terms of kriging metamodels and a set of auxiliary variable vectors. The fundamental property of the sub-problem is that it can be fully constructed from the results obtained from a single run, in a fixed point of the design space, of the simulation-based performance assessment model. This ensures the scalability of the sub-problem to high-dimensional spaces of design variables. By solving a sequence of sub-problems, each formulated in the solution of the previous, a solution to the original ε-constraint problem is obtained, therefore providing estimates of the Pareto optimal set of the original bi-objective optimization problem. To illustrate the framework, sets of Pareto optimal designs were obtained for a 37-story moment resisting frame with 259 discrete design variables and subject to wind tunnel informed stochastic wind loads. The efficiency and strong convergence properties of the proposed approach were demonstrated.

Acknowledgments

Support for this work was in part provided by the National Science Foundation through Grant No. CMMI-1462084 and CMMI-1750339.

Appendix A. The Auxiliary Variable Vectors

To derive the AVVs in the current design point $\tilde{\mathbf{x}}$, it is first necessary to consider the following variable that can be defined for each realization of $\mathbf{U}$:

$$\boldsymbol{\Upsilon}_k(\mathbf{u},\tilde{\mathbf{x}}) = \mu_{\mathbf{F}}(\mathbf{u},\tilde{\mathbf{x}}) + \frac{[edp_k(\mathbf{u},\tilde{\mathbf{x}}) - \mu_{r_k}(\mathbf{u},\tilde{\mathbf{x}})]\mathbf{C}_{\mathbf{F}}(\mathbf{u},\tilde{\mathbf{x}})\boldsymbol{\Gamma}_{r_k}(\tilde{\mathbf{x}})}{\sigma^2_{r_k}(\mathbf{u},\tilde{\mathbf{x}})} \tag{A.1}$$

where μ_{r_k} and σ_{r_k} are the mean and standard deviation of the component response process of Eq. (6) respectively while $\mu_{\mathbf{F}}$ and $\mathbf{C}_{\mathbf{F}}$ are the mean and the covariance matrix of the following vector-valued stochastic process:

$$\mathbf{F}(t;\mathbf{u},\tilde{\mathbf{x}}) = s_1\left[\mathbf{f}(t;\mathbf{u}) + \mathbf{K}(\tilde{\mathbf{x}})\boldsymbol{\Phi}_M(\tilde{\mathbf{x}})\mathbf{q}_{r_M}(t;\mathbf{u},\tilde{\mathbf{x}})\right] \tag{A.2}$$

The interest in defining $\boldsymbol{\Upsilon}_k$, is that when this variable is multiplied with the influence function $\Gamma^T_{r_k}$, the following static relationship holds:

$$edp_k(\mathbf{u},\tilde{\mathbf{x}}) = \boldsymbol{\Gamma}^T_{r_k}(\tilde{\mathbf{x}})\boldsymbol{\Upsilon}_k(\mathbf{u},\tilde{\mathbf{x}}) \tag{A.3}$$

The advantage of Eq. (A.3) is that it provides an exact static relationship between the nominal system and the engineering demand parameter, EDP_k. To this end, the following AVVs can be defined as:

$$\widehat{\boldsymbol{\Upsilon}}_k(\tilde{\mathbf{x}}) = \mu_{\boldsymbol{\Upsilon}_k}(\tilde{\mathbf{x}}) \tag{A.4}$$

$$\check{\boldsymbol{\Upsilon}}_k(\tilde{\mathbf{x}}) = \frac{\mathbf{C}_{\boldsymbol{\Upsilon}_k}(\tilde{\mathbf{x}})\boldsymbol{\Gamma}_{r_k}(\tilde{\mathbf{x}})}{\sigma_{EDP_k}(\tilde{\mathbf{x}})} \tag{A.5}$$

where $\mu_{\boldsymbol{\Upsilon}_{d_k}}$ and $\mathbf{C}_{\boldsymbol{\Upsilon}_{d_k}}$ are the mean and covariance matrix of $\boldsymbol{\Upsilon}_k$ respectively.

The significance of the AVVs lays in the fact that when $\widehat{\boldsymbol{\Upsilon}}_k$ and $\check{\boldsymbol{\Upsilon}}_k$ are statically applied to the nominal structure with stiffness $\mathbf{K}$, the resulting responses in r_k coincide with the expected value and the standard deviation of the engineering demand parameter, EDP_k. In other words, the following holds:

$$\mu_{EDP_k}(\tilde{\mathbf{x}}) = \boldsymbol{\Gamma}^T_{r_k}(\tilde{\mathbf{x}})\widehat{\boldsymbol{\Upsilon}}_k(\tilde{\mathbf{x}}) \tag{A.6}$$

$$\sigma_{EDP_k}(\tilde{\mathbf{x}}) = \boldsymbol{\Gamma}^T_{r_k}(\tilde{\mathbf{x}})\check{\boldsymbol{\Upsilon}}_k(\tilde{\mathbf{x}}) \tag{A.7}$$

where, the relationships are exact at the current design point $\tilde{\mathbf{x}}$.

Appendix B. Sensitivity Analysis

The partial derivative of the performance constraint $\widehat{L}$ with respect to the jth component of $\mathbf{x}$ can be obtained as:

$$\begin{aligned}\frac{\partial \widehat{L}(\mathbf{x})}{\partial x_j} = &\sum_{k=1}^{N_g}\left(\frac{\partial \widehat{\mu}_{DV_k}}{\partial \mu_{EDP_k}}\frac{\partial \mu_{EDP_k}(\mathbf{x})}{\partial x_j} + \frac{\partial \widehat{\mu}_{DV_k}}{\partial \sigma_{EDP_k}}\frac{\partial \sigma_{EDP_k}(\mathbf{x})}{\partial x_j}\right) + \frac{\alpha}{2\cdot \mathrm{Std}[DV(\mathbf{x})]}\left[\sum_{k=1}^{N_g}\sum_{m=1}^{N_g}\rho_{km}(\tilde{\mathbf{x}})\cdot\left(\widehat{\sigma}_{DV_m}(\mathbf{x})\left(\frac{\partial \widehat{\sigma}_{DV_k}}{\partial \mu_{EDP_k}}\frac{\partial \mu_{EDP_k}(\mathbf{x})}{\partial x_j} + \frac{\partial \widehat{\sigma}_{DV_k}}{\partial \sigma_{EDP_k}}\frac{\partial \sigma_{EDP_k}(\mathbf{x})}{\partial x_j}\right)\right.\right.\\ &\left.\left. + \widehat{\sigma}_{DV_k}(\mathbf{x})\left(\frac{\partial \widehat{\sigma}_{DV_m}}{\partial \mu_{EDP_m}}\frac{\partial \mu_{EDP_m}(\mathbf{x})}{\partial x_j} + \frac{\partial \widehat{\sigma}_{DV_m}}{\partial \sigma_{EDP_m}}\frac{\partial \sigma_{EDP_m}(\mathbf{x})}{\partial x_j}\right)\right)\right]\end{aligned} \tag{B.1}$$

where $\widehat{\mu}_{DV_k}$ and $\widehat{\sigma}_{DV_k}$ are explicit functions of μ_{EDP_k} and σ_{EDP_k}; while $\frac{\partial \mu_{EDP_k}(\mathbf{x})}{\partial x_j}$ and $\frac{\partial \sigma_{EDP_k}(\mathbf{x})}{\partial x_j}$ are given by:

$$\frac{\partial \mu_{EDP_k}(\mathbf{x})}{\partial x_j} \approx \frac{\partial \boldsymbol{\Gamma}^T_{r_k}(\mathbf{x})}{\partial x_j}\widehat{\boldsymbol{\Upsilon}}_k(\tilde{\mathbf{x}}) \tag{B.2}$$

$$\frac{\partial \sigma_{EDP_k}(\mathbf{x})}{\partial x_j} \approx \frac{\partial \boldsymbol{\Gamma}^T_{r_k}(\mathbf{x})}{\partial x_j}\check{\boldsymbol{\Upsilon}}_k(\tilde{\mathbf{x}}) \tag{B.3}$$

where the partial derivatives of the influence functions $\boldsymbol{\Gamma}_{r_k}$ can be obtain through classic approaches (Chan et al., 1995; Spence and Gioffrè, 2011).

Appendix C. Wind speed transformation scheme

The design wind speed at the site of interest, $\overline{V}_H$, can be obtained by transforming the extreme wind speed, $\overline{v}_y$, averaged over a time interval τ at a meteorological station, to the site-specific wind speed, $\overline{V}_H$, through the following probabilistic transformation model based on the Logarithmic Law (Minciarelli et al., 2001):

$$\overline{v}_H(\mathbf{u}_w, T, z_0) = e_7 e_3(\tau, T)\left(\frac{e_5 z_0}{e_6 z_{01}}\right)^{e_4\delta}\frac{\ln[H/(e_5 z_0)]}{\ln[H_{met}/(e_6 z_{01})]}e_2 e_1 \overline{v}_y(\tau, H_{met}, z_{01}) \tag{C.1}$$

where z_0 is the roughness length at the site of interest; z_{01} and H_{met} are the roughness length and height at the meteorological station; δ is an empirical constant taken as $\delta = 0.0706$; and E_1, to E_7 are uncertain parameters collected in $\mathbf{U}_E$. Specifically, E_1 and E_2 account for observational and sampling errors in collecting the meteorological wind speeds; E_4, E_5, and E_6 model the uncertainties associated with the actual values of δ and of the roughness lengths z_0 and z_{01}; $E_3(\tau, T)$ is the conversion factor that accounts for the errors in converting between wind speed averaging times; while E_7 is a model uncertainty to be used in the case of hurricanes and tornadoes. Possible marginal distributions for the elements of vector $\mathbf{U}_E$ are given in Table C3.

Table C.3
Possible marginal distributions for the elements of vector $\mathbf{U}_E$

Variable	Mean	C.O.V.	Distribution	Ref.
E_1	1	0.1	Trunc. Normal	Minciarelli et al. (2001)
E_2	1	0.025	Normal	Diniz et al. (2004)
E_3	[a]	0.075	Normal	Diniz et al. (2004)
E_4	1	0.1	Trunc. Normal	Diniz et al. (2004)
E_5	1	0.3	Trunc. Normal	Diniz et al. (2004)
E_6	1	0.3	Trunc. Normal	Diniz et al. (2004)
E_7	1	0.05	Normal	Diniz et al. (2004)

[a] Dependent on averaging times τ and T.

References

Baker, J.W., Cornell, C.A., 2008. Uncertainty propagation in probabilistic seismic loss estimation. Struct. Saf. 30, 236–252.
Barbato, M., Petrini, F., Unnikrishnan, V.U., Ciampoli, M., 2013. Performance-based hurricane engineering (PBHE) framework. Struct. Saf. 45, 24–35.
Bashor, R., Kijewski-Correa, T., Kareem, A., 2005. On the wind-induced response of tall buildings: the effect of uncertainties in dynamic properties and human comfort thresholds. In: Proc., 10th Americas Conf. On Wind Engineering (CD-ROM).
Bernardini, E., Spence, S.M.J., Gioffrè, M., 2012. Dynamic response estimation of tall buildings with 3D modes: a probabilistic approach to the high frequency force balance method. J. Wind Eng. Ind. Aerod. 104–106, 56–64.
Bernardini, E., Spence, S.M.J., Kwon, D.-K., Kareem, A., 2015. Performance-based design of high-rise buildings for occupant comfort. J. Struct. Eng. 141. https://doi.org/10.1061/(ASCE)ST.1943-541X.0001223.
Bernardini, E., Spence, S.M.J., Wei, D., Kareem, A., 2015. Aerodynamic shape optimization of civil structures: a CFD-enabled kriging-based approach. J. Wind Eng. Ind. Aerod. 144, 154–164.
Bezabeh, M.A., Bitsuamlak, G.T., Popovski, M., Tesfamariam, S., 2018. Probabilistic serviceability-performance assessment of tall mass-timber buildings subjected to stochastic wind loads: Part ii - structural reliability analysis. J. Wind Eng. Ind. Aerod. 181, 112–125.
Bobby, S., Spence, S.M.J., Kareem, A., 2017. Data-driven performance-based topology optimization of uncertain wind-excited tall buildings. Struct. Multidiscip. Optim. 54, 13791402.
Bocchini, P., Frangopol, D.M., 2012. Optimal resilience- and cost-based post disaster intervention prioritization for bridges along a highway segment. J. Bridge Eng. 17, 117–129.
Carmichael, D., 1980. Computation of pareto optima in structural design. Int. J. Numer. Methods Eng. 15, 925–929.
Chan, C.M., Grierson, D.E., Sherbourne, A.N., 1995. Automatic optimal design of tall steel building frameworks. J. Struct. Eng. 121, 838–847.
Chen, X., Kareem, A., 2005. Proper orthogonal decomposition-based modeling, analysis, and simulation of dynamic wind load effects on structures. J. Eng. Mech. 131, 325–339.
Chuang, W., Spence, M.J., 2017. A performance-based design framework for the integrated collapse and non-collapse assessment of wind excited buildings. Eng. Struct. 150, 746–758.
Cui, W., Caracoglia, L., 2018. A unified framework for performance-based wind engineering of tall buildings in hurricane-prone regions based on lifetime intervention-cost estimation. Struct. Saf. 73, 75–86.
Ding, F., Kareem, A., 2018. A multi-fidelity shape optimization via surrogate modeling for civil structures. J. Wind Eng. Ind. Aerod. 178, 49–56.
Diniz, S.M.C., Sadek, F., Simiu, E., 2004. Wind speed estimation uncertainties: effects of climatological and micrometeorological parameters. Probabilist. Eng. Mech. 19, 361–371.
Du, X., Chen, W., 2004. Sequential optimization and reliability assessment method for efficient probabilistic design. ASME J. Mech. Des. 126, 225–233.
Elshaer, A., Bitsuamlak, G., 2018. Multiobjective aerodynamic optimization of tall building openings for wind-induced load reduction. J. Struct. Eng. 144.
Federal Emergency Management Agency (FEMA), 2012a. Seismic Performance Assessment of Buildings, vol. 1. FEMA Publication P-58-1, Washington, DC. Methodology.
Federal Emergency Management Agency (FEMA), 2012b. Seismic Performance Assessment of Buildings, Volume 3 Supporting Electronic Materials and Background Documentation. FEMA Publication P-58-3, Washington, DC.
Forrester, A., Keane, A., et al., 2008. Engineering Design via Surrogate Modelling: a Practical Guide. John Wiley & Sons.
Fragiadakis, M., Lagaros, N.D., Papadrakakis, M., 2006. Performance-based multiobjective optimum design of steel structures considering life-cycle cost. Struct. Multidiscip. Optim. 32, 111.
Fu, G., Frangopol, D.M., 1990. Reliability-based vector optimization of structural systems. J. Struct. Eng. 116, 2143–2161.
Garcıa-Segura, T., Yepes, V., Frangopol, D.M., 2017. Multi-objective design of post-tensioned concrete road bridges using artificial neural networks. Struct. Multidiscip. Optim. 56, 139150.
Gencturk, B., 2013. Multiobjective optimization for performance-based seismic design of steel moment frame structures. Earthq. Eng. Struct. Dyn. 42, 6179.
Gidaris, I., Taflanidis, A.A., 2015. Performance assessment and optimization of fluid viscous dampers through lifecycle cost criteria and comparison to alternative design approaches. Bull. Earthq. Eng. 13.
Gidaris, I., Taflanidis, A.A., Mavroeidis, G.P., 2018. Multiobjective design of supplemental seismic protective devices utilizing lifecycle performance criteria. J. Struct. Eng. 144.
Ierimonti, L., Caracoglia, L., Venanzi, I., Materazzi, A.L., 2017. Investigation on life-cycle damage cost of wind-excited tall buildings considering directionality effects. J. Wind Eng. Ind. Aerod. 171, 207–218.
Ierimonti, L., Venanzi, I., Caracoglia, L., 2018. Life-cycle damage-based cost analysis of tall buildings equipped with tuned mass dampers. J. Wind Eng. Ind. Aerod. 176, 54–64.
Jensen, H.A., Valdebenito, M.A., Schuëller, G.I., 2008. An efficient reliability-based optimization scheme for uncertain linear systems subject to general Gaussian excitation. Comput. Methods Appl. Mech. Eng. 198, 72–87.
Jensen, H.A., Kusanovic, D.S., Valdebenito, M.A., Schuëller, G.I., 2012. Reliability-based design optimization of uncertain stochastic systems: gradient-based scheme. J. Eng. Mech. 138, 60–70.
Jia, G., Taflanidis, A.A., 2013. Non-parametric stochastic subset optimization for optimal-reliability design problems. Comput. Struct. 126, 86–99.
Jia, G., Taflanidis, A.A., Beck, J.L., 2015. Non-parametric stochastic subset optimization for design problems with reliability constraints. Struct. Multidiscip. Optim. 52, 1185–1204.
Kim, B., Tse, K.T., Tamura, Y., 2018. POD analysis for aerodynamic characteristics of tall linked buildings. J. Wind Eng. Ind. Aerod. 181, 126–140.

Li, Y., Kareem, A., 1993. Simulation of multivariate random processes: Hybrid DFT and digital filtering approach. J. Eng. Mech. 119, 1078–1098.
Liu, M., Burns, S.A., Wen, Y.K., 2005. Life-cycle cost assessment of rc and ecc frames using structural optimization. Earthq. Eng. Struct. Dyn. 34, 289306.
Marler, R., Arora, J., 2004. Survey of multi-objective optimization methods for engineering. Struct. Multidiscip. Optim. 26, 369–395.
Mavrotas, G., 2009. Effective implementation of the ε-constraint method in multi-objective mathematical programming problems. Appl. Math. Comput. 213, 455–465.
Minciarelli, F., Gioffrè, M., Grigoriu, M., Simiu, E., 2001. Estimates of extreme wind effects and wind load factors: influence of knowledge uncertainties. Probabilist. Eng. Mech. 16, 331–340.
Morris, M.D., Mitchell, T.J., 1995. Exploratory designs for computational experiments. J. Stat. Plan. Inference 43, 381–402.
Muñoz Paniagua, J., García, J., 2019. Aerodynamic surrogate-based optimization of the nose shape of a high-speed train for crosswind and passing-by scenarios. J. Wind Eng. Ind. Aerod. 184, 139–152.
National Institute of Standards and Technology, 2016. Extreme wind speed data sets: hurricane wind speeds. https://www.itl.nist.gov/div898/winds/hurricane.htm.
Ouyang, Z., Spence, S.M.J., 2019. A performance-based damage estimation framework for the building envelope of wind-excited engineered structures. J. Wind Eng. Ind. Aerod. 186, 139–154.
Peng, L., Huang, G., Chen, X., Kareem, A., 2017. Simulation of multivariate nonstationary random processes: Hybrid stochastic wave and proper orthogonal decomposition approach. J. Eng. Mech. 143.
Ruan, D., He, H., Castañón, D.A., Mehta, K.C., 2006. Normalized proper orthogonal decomposition (NPOD) for building pressure data compression. J. Wind Eng. Ind. Aerod. 94, 447–461.
Saadat, S., Camp, C.V., Pezeshk, S., 2014. Seismic performance-based design optimization considering direct economic loss and direct social loss. Eng. Struct. 76, 193–201.
Sack, J., Welch, W., Mitchell, T., Wynn, H., 1989. Design and analysis of computer experiments (with discussion). Stat. Sci. 4, 409–435.
Schuëller, G.I., Jensen, H.A., 2008. Computational methods in optimization considering uncertainties - an overview. Comput. Methods Appl. Mech. Eng. 198, 2–13.
Spence, S.M.J., Gioffrè, M., 2011. Efficient algorithms for the reliability optimization of tall buildings. J. Wind Eng. Ind. Aerod. 99, 691–699.
Spence, S.M.J., Gioffrè, M., Kareem, A., 2016. An efficient framework for the reliability-based design optimization of large-scale uncertain and stochastic linear systems. Probabilist. Eng. Mech. 44, 174–182.
Suksuwan, A., Spence, S.M., 2018. Efficient approach to system-level reliability-based design optimization of large-scale uncertain and dynamic wind-excited systems. ASCE-ASME J. Risk Uncertainty Eng. Syst., Part A: Civ. Eng. 4.
Suksuwan, A., Spence, S.M.J., 2018. Optimization of uncertain structures subject to stochastic wind loads under system-level first excursion constraints: a data-driven approach. Comput. Struct. 210, 58–68.
Taflanidis, A.A., Beck, J.L., 2009. Stochastic subset optimization for reliability optimization and sensitivity analysis in system design. Comput. Struct. 87, 318–331.
Tokyo Polytechnic University, 2008. TPU Wind Pressure Database. http://wind.arch.t-kougei.ac.jp/system/eng/contents/code/tpu.
Tootkaboni, M., Asadpoure, A., Guest, J.K., 2012. Topology optimization of continuum structures under uncertainty-a polynomial chaos approach. Comput. Methods Appl. Mech. Eng. 201, 263–275.
Valdebenito, M.A., Schuëller, G.I., 2010. A survey on approaches for reliability-based optimization. Struct. Multidiscip. Optim. 42, 645–663.
Xu, J., Spencer, B.F., Lu, X., Chen, X., Lu, L., 2017. Optimization of structures subject to stochastic dynamic loading. Comput. Aided Civ. Infrastruct. Eng. 32, 657–673.
Zhang, W., Reimann, M., 2014. A simple augmented ε-constraint method for multi-objective mathematical integer programming problems. Eur. J. Oper. Res. 234, 15–24.
Zheng, X.W., Li, H.N., Li, C., 2019. Damage probability analysis of a high-rise building against wind excitation with recorded field data and direction effect. J. Wind Eng. Ind. Aerod. 184, 10–22.
Zou, T., Mahadevan, S., 2006. A direct decoupling approach for efficient reliability-based design optimization. Struct. Multidiscip. Optim. 31, 190–200.